I&EC research
Industrial & Engineering Chemistry Research

Article

pubs.acs.org/IECR

Nonuniform External Filter Cake in Long Injection Wells

Azim Kalantariasl,[†] Rouhi Farajzadeh,[‡,§] Zhenjiang You,[*,†] and Pavel Bedrikovetsky[†]

[†]Australian School of Petroleum, University of Adelaide, Adelaide, South Australia 5005, Australia

[‡]Delft University of Technology, Stevinweg 1, 2628 CN Delft, The Netherlands

[§]Shell International Global Solutions, 2280 AB Rijswijk, The Netherlands

Supporting Information

ABSTRACT: Buildup and stabilization of external filter cake is a well-known phenomenon in several environmental and industrial applications. Significant decline of the tangential rate along thick intervals in lengthy vertical wells yields a nonuniform external filter cake profile. We derive the mechanical equilibrium equations for the stabilized cake profile accounting for electrostatic particle−rock interaction, varying permeate factor, applying the torque balance to describe cake equilibrium, and calculating the lever arm ratio using Hertz's theory for contact deformation of cake and particles. An implicit formula for the cake thickness along the well is derived. Two regimes of the stabilized cake buildup correspond to low rates, where the cake starts from the reservoir top, and for high rates, where the cake is formed in the lower well section only. The sensitivity analysis shows that the drag and permeate forces are the competitive factors affecting cake thickness under varying Young's modulus, rate, and salinity. The main parameters defining external cake profile are injection rate, cake porosity, water salinity, and Young's modulus.

1. INTRODUCTION

Well-injectivity decline has been widely reported for fresh and hot water storage in aquifers, for industrial waste disposal, during well drilling and completion, for sea- and produced-water injection into oilfields, and geothermal reservoirs.[1−7] The phenomenon is explained by deep bed filtration of solid and liquid particles associated with the injected fluids causing permeability decline. In addition, the formation of external filter cake on the sand-face wall causes additional hydraulic resistance to the injected water. Similar processes occur during well drilling and completion.[5,6]

The decision making, planning, and design of the above environmental and petroleum production processes, determining optimal particle sizes, concentrations, injection rates, etc., strongly depend on the results of laboratory-based mathematical modeling.

For the case of low concentration of the retained particles, the filtration and formation damage coefficients are constant, the governing equations are linear, and the problem for axi-symmetric suspension injection with low retention concentration allows for exact analytical solution.[8−12] The suspension concentration around the well is steady state, yielding linear growth of the retained concentration and the pressure drawdown with time under constant injection rate. The model parameters, which are necessary for well behavior prediction, can be determined from the so-called three-point-pressure corefloods.[13]

More sophisticated mathematical models for suspension−colloidal transport in porous media include random-walk equations,[14−17] population-balance models,[18−22] trajectory analysis,[23,24] and direct pore scale simulation.[25]

Incompressibility of the external cake results in the analytical model, predicting linear growth of pressure drop versus the amount of injected particles.[11,13,26] Cake compressibility and particle recompaction in the cake in the course of the pressure drawdown increase cause nonlinear pressure drawdown growth.[27,28]

Cake stabilization after a transient buildup has been observed during well drilling. To model this phenomenon, force balance and torque balance models for the cake mechanical equilibrium have been utilized.[5,6,29−31]

It was found that stabilized cake thickness and consequent well index are strongly rate-dependent.[32] The tangential rate in long vertical wells in thick reservoirs declines from the injected value on the reservoir top to zero at the bottom. Therefore, stabilized cake thickness and overall hydraulic resistance significantly increase with depth. However, the works reported in refs 32 and 33 consider a constant thickness cake in "short" wells only.

Nonuniform cake thickness on the wall of a long vertical injector is modeled in ref 34. However, the electrostatic force, which is dominant with injection of high salinity water, is ignored. The permeate factor is assumed to be constant, which can vary significantly.[35] The model uses the force balance as a mechanical equilibrium condition, resulting in introduction of the friction force with the empirically determined Coulomb friction coefficient, which is not always available. The model has been solved numerically. The analogous work for nonuniform cake in fractured well is presented in ref 36.

The mathematical model for nonuniform cake profile in long wells, presented in the current work, is free of the above-mentioned shortcomings. The electrostatic force as calculated using the Derjaguin−Landau−Verwey−Overbeek (DLVO) theory is included in the microscale particle−cake interaction model and is proven to be one of the dominant forces. The

Received: December 19, 2014
Revised: March 1, 2015
Accepted: March 1, 2015
Published: March 2, 2015

DOI: 10.1021/ie504936q
Ind. Eng. Chem. Res. 2015, 54, 3051−3061

varying permeate factor is included in the model; the modeling exhibits its high effect on the cake profile. Using the torque balance for mechanical equilibrium of the external cake and calculating the contact particle−grain area using Hertz's theory allows the reduction of the number of empirical model constants by one if compared with the force−balance model. Other eliminations of the model parameters come from neglecting the lifting force and small contact particle−cake deformation areas typical for sandstones. Despite not adopting several simplifying assumptions of refs 34 and 36, an analytical model is derived for calculation of the cake thickness. It was found that depending on the injection rate, the cake can be formed on the overall well surface or only on its lower part.

The structure of the present paper is as follows. Section 2 presents the torque balance as the mechanical equilibrium condition for stabilized cake. Equations for varying cake profile are derived in section 3 from the torque balance and mass conservation. The equations are solved analytically in section 4, allowing for multivariant sensitivity study in section 5. The discussion of main parameters defining the cake profile form and the model applicability concludes the paper.

2. MECHANICAL EQUILIBRIUM OF STABILIZED CAKE

A particle on the cake surface with streamlines of the injected water in the well column is shown in Figures 1 and 2. Water enters the reservoir with simultaneous placement of suspended particles on the cake surface. The deposited particle is subject to the electrostatic, drag, permeate, lifting, and gravitational forces, denoted by F_e, F_d, F_p, F_l, and F_g, respectively.[32,37,38] In the case of rolling, the external moment of surface stress M_E adds to the detaching torques. The torques of electrostatic and permeate forces attach the particle to the cake surface while the drag, gravitational, lifting, and external stress torques detach the particle.

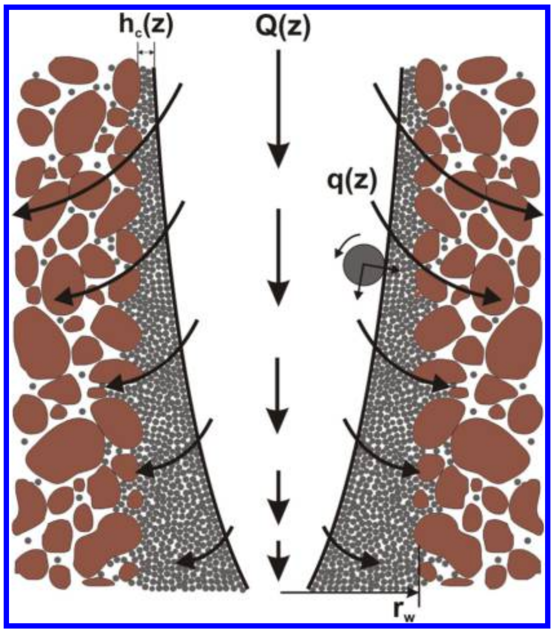

Figure 1. Schematic of nonuniform external filter cake profile.

The condition of mechanical equilibrium of the particle on the cake surface is the equality of the detaching and attaching torques

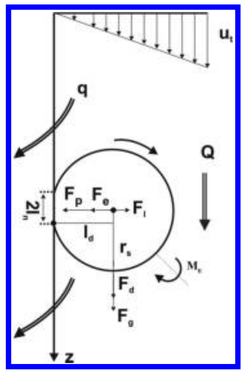

Figure 2. Schematic of forces and lever arms at particle dislodgment moment.

$$(F_d + F_g)l_d + M_E = (F_p + F_e)l_n \tag{1}$$

which correspond to the left- and right-hand sides of eq 1, respectively. Here, l_d and l_n are lever arms for detaching and attaching (normal) forces, respectively (see Figure 2).

For typical values of well rates and particle sizes, the lifting force is negligible if compared with other forces, so it is not accounted for in mechanical equilibrium eq 1. The expressions for the above forces and torques are presented in Appendix S1 of Supporting Information. The electrostatic forces depend on the separation distance between the particle and surface, see eqs S-2−S-4 in Supporting Information. If the attaching torque exceeds the detaching torque, the separation distance decreases until equilibrium (eq 1) is established. The increase of the detaching torque, where it is lower than the attaching torque with the maximum value of the electrostatic force, increases the separation distance until the new equilibrium. If the detaching torque exceeds the attaching torque with the maximum value of the electrostatic force, the particle leaves the cake and starts rolling along the cake surface. Therefore, the condition of the cake mechanical equilibrium is eq 1 with the maximum value of the electrostatic attractive force (F_e).

We now consider mutual deformation of the particle and the rock under the attachment condition (Figure 2). The deforming force is the total of electrostatic and permeate forces. The radius of the contact area, l_n, is determined from Hertz's theory[6,39−42]

$$l_n = \left(\frac{(F_p + F_e)r_s}{K}\right)^{1/3} \tag{2}$$

where the composite Young's modulus, K, depends on the Poisson's ratio, σ, and Young's modulus, E, of the particle and of the cake:

$$K = \frac{4}{3\pi}\left(\frac{(1-\sigma_s^2)}{\pi E_s} + \frac{(1-\sigma_c^2)}{\pi E_c}\right)^{-1} = \frac{2}{3}\left(\frac{1-\sigma^2}{E}\right)^{-1} \tag{3}$$

Here, subscripts s and c refer to particle and cake, respectively.

Schechter shows that for rigid particles like silica or quartz, the radius of the contact area is significantly smaller than the particle radius.[6] Therefore, further in the text, the detaching lever arm, l_d, is assumed to be equal to the particle radius (see Figure 2).

DOI: 10.1021/ie504936q
Ind. Eng. Chem. Res. 2015, 54, 3051−3061

3. EQUATIONS FOR CAKE PROFILE $h_C(Z)$

Let us derive equations for the stabilized cake profile. The main assumptions are incompressibility of the fluid, rock, and cake; torque balance as a mechanical equilibrium condition for the particle on the rock surface; linear kinetics equation for the particle injected fluid with the constant filtration coefficient; and constant formation−damage coefficient.[5−7,21]

The difference between tangential flow rates, Q, in two cross sections along the well is equal to water volume injected through the interval between the cross sections. Therefore, the volume balance for incompressible fluid is

$$\frac{\mathrm{d}Q}{\mathrm{d}z} = -q\Big|_{r_w - h_c(z)} \tag{4}$$

where q is the flow rate per unit length of the reservoir, r_w the well radius, and h_c the cake thickness.

Using the eq S-9 in Supporting Information for external moment M_E, and substituting the expression for contact area radius l_n (eq 2) along with the assumption that $l_d = r_s$ into torque balance eq 1 yields

$$\left(1.4\frac{F_d}{F_e} + \frac{F_g}{F_e}\right) = \left(\frac{F_p}{F_e} + 1\right)^{4/3}\left(\frac{F_e r_s}{K r_s^3}\right)^{1/3} \tag{5}$$

The dimensionless parameters for tangential flow rate, cake thickness, and reservoir thickness are defined as

$$\tilde{Q} = \frac{Q(z)}{Q_0}, \quad \tilde{h}_c = \frac{h_c(z)}{r_w}, \quad \tilde{z} = \frac{z}{H_f} \tag{6}$$

respectively, where Q_0 is the injection rate and H_f is the thickness of reservoir. Substituting expressions for drag, gravitational, and permeate forces (eqs S-8−S-13 in Supporting Information) and expression for permeate rate (S-23) into eq 5 yields the following dimensionless relationship:

$$\left(\frac{1.4 \times 4\omega\pi\mu r_s^2\tilde{Q}Q_0}{\pi r_w^3(1-\tilde{h}_c)^3F_e} + \frac{4}{3F_e}\pi r_s^3\Delta\rho g\right) = \left(\frac{6\pi\mu r_s 0.36\left(\frac{k_c}{r_s^2}\right)^{-2/5}}{2\pi r_w(1-\tilde{h}_c)F_e}\frac{2\pi k_c\Delta p}{\mu\left[-\ln(1-\tilde{h}_c) + (1+mt_{tr})\ln\left(\frac{r_e}{r_w}\right)\frac{k_c}{k}\right]} + 1\right)^{4/3}\left(\frac{F_e r_s}{K r_s^3}\right)^{1/3} \tag{7}$$

Expressing the dimensionless tangential flow rate, $\tilde{Q}$, from torque balance eq 7 yields

$$\tilde{Q} = \left(\frac{2.16\pi r_s^{9/5}k_c^{3/5}F_e^{-1}r_w^{-1}\Delta p}{(1-\tilde{h}_c)\left[-\ln(1-\tilde{h}_c) + (1+mt_{tr})\ln\left(\frac{r_e}{r_w}\right)\frac{k_c}{k}\right]} + 1\right)^{4/3}\frac{F_e^{4/3}r_s^{-8/3}K^{-1/3}r_w^{3}}{5.6\omega\mu Q_0}(1-\tilde{h}_c)^3 - \frac{\pi\Delta\rho g r_s r_w^3}{4.2\omega\mu Q_0}(1-\tilde{h}_c)^3 \tag{8}$$

Introduction of dimensionless constants A, B, C, and D significantly simplifies eq 8 as

$$\tilde{Q} = C\left(\frac{A}{(1-\tilde{h}_c)(-\ln(1-\tilde{h}_c) + B)} + 1\right)^{4/3}(1-\tilde{h}_c)^3 - D(1-\tilde{h}_c)^3 \tag{9}$$

where the four dimensionless groups are

$$A = 2.16\pi r_s^{9/5}k_c^{3/5}F_e^{-1}r_w^{-1}\Delta p$$

$$B = (1 + mt_{tr})\ln\left(\frac{r_e}{r_w}\right)\frac{k_c}{k}$$

$$C = \frac{F_e^{4/3}K^{-1/3}r_s^{-8/3}r_w^{3}}{5.6\omega\mu Q_0}$$

$$D = \frac{\pi\Delta\rho g r_s r_w^3}{4.2\omega\mu Q_0} \tag{10}$$

Substitution of the permeate rate expression (eq S-23 in Supporting Information) into volumetric balance eq 4 results in

$$\frac{\mathrm{d}\tilde{Q}}{\mathrm{d}\tilde{z}} = -\frac{2\pi k_c H_f}{Q_0\mu}\frac{\Delta p}{[-\ln(1-\tilde{h}_c) + B]}$$

$$\frac{\mathrm{d}\tilde{Q}}{\mathrm{d}\tilde{z}} = -\frac{G}{[-\ln(1-\tilde{h}_c) + B]}, \quad G = \frac{2\pi k_c H_f}{Q_0\mu}\Delta p \tag{11}$$

Substituting the tangential rate expression (eq 9) into volumetric balance equation (eq 11) results in the following ordinary differential equation:

$$\frac{\mathrm{d}}{\mathrm{d}\tilde{z}}\left\{C\left(\frac{A}{(1-\tilde{h}_c)(-\ln(1-\tilde{h}_c) + B)} + 1\right)^{4/3}(1-\tilde{h}_c)^3 - D(1-\tilde{h}_c)^3\right\} = -\frac{G}{[-\ln(1-\tilde{h}_c) + B]} \tag{12}$$

The obtained ordinary differential equation (eq 12) determines the dimensionless cake thickness profile $\tilde{h}_c(z)$. The formulas for the cake thickness profile, based on solutions of eq 12, are derived in the next section.

4. EXPRESSIONS FOR CAKE PROFILES

Let us introduce the critical injection rate resulting in zero cake thickness on the well wall. The critical rate is determined from eq 9 as

$$\tilde{Q}_{cr} = C\left(\frac{A}{B} + 1\right)^{4/3} - D \tag{13}$$

Let us first consider the case in which the injection rate is below its critical value. In this case, $\tilde{Q}$ is equal to one on the left-hand side of eq 9, which determines cake thickness at the top of the reservoir:[32]

$$1 = C\left(\frac{A}{(1-\tilde{h}_{c0})(-\ln(1-\tilde{h}_{c0}) + B)} + 1\right)^{4/3}(1-\tilde{h}_{c0})^3 - D(1-\tilde{h}_{c0})^3 \tag{14}$$

DOI: 10.1021/ie504936q
Ind. Eng. Chem. Res. 2015, 54, 3051−3061

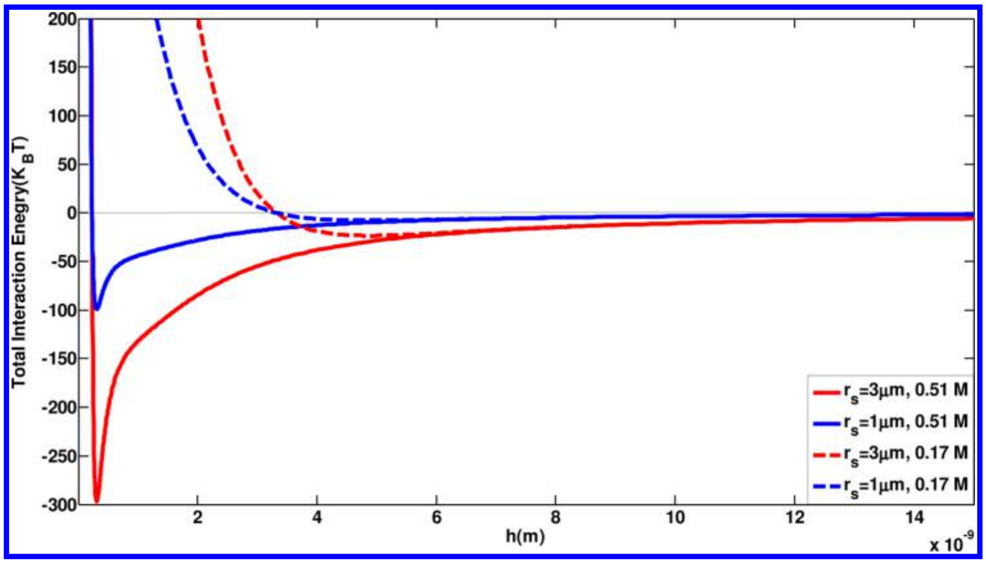

Figure 3. Total electrostatic interaction energy: $A_{132} = 2 \times 10^{-21}$ J, ζ potential values are −12 and −27 mV for salinities 0.51 and 0.17 M, respectively.

It provides the initial condition (boundary value) for the ordinary differential equation in eq 12:

$$\tilde{z} = 0: \quad \tilde{h}_c = \tilde{h}_{c0} \tag{15}$$

Separating variables in the ordinary differential equation in eq 12 and integrating both sides accounting for initial condition given in eq 15 yields

$$\tilde{z} = \frac{1}{G}\left\{\frac{4C}{3}\int_{\tilde{h}_c}^{\tilde{h}_{c0}}\left(\frac{A(-\ln(1-\tilde{h}_c)+B-1)}{(1-\tilde{h}_c)^2(-\ln(1-\tilde{h}_c)+B)}\right)\left(\frac{A}{(1-\tilde{h}_c)(-\ln(1-\tilde{h}_c)+B)}+1\right)^{1/3}(1-\tilde{h}_c)^3\,d\tilde{h}_c - 3\int_{\tilde{h}_c}^{\tilde{h}_{c0}}\left[C\left(\frac{A}{(1-\tilde{h}_c)(-\ln(1-\tilde{h}_c)+B)}+1\right)^{4/3} - D\right][-\ln(1-\tilde{h}_c)+B](1-\tilde{h}_c)^2\,d\tilde{h}_c\right\} \tag{16}$$

Equation 16 provides the implicit expression for the cake profile $\tilde{h}_c(z)$, in which the constant $\tilde{h}_{c0}$ is determined from transcendental eq 14.

Now let us discuss the case in which the injection rate is above its critical value. In this case, the cake thickness remains zero from the reservoir top down, until the depth z_{cr} where the tangential rate reaches the critical value. First, we determine how the tangential rate decreases with depth under the absence of the cake. Substituting eq S-23 in Supporting Information into eq 4 and applying dimensionless variables (eq 6) yield

$$\frac{d\tilde{Q}}{d\tilde{z}} = -\frac{2\pi k H_f}{\mu Q_0(1+mt_{tr})}\frac{\Delta p}{\ln\frac{r_e}{r_w}} \tag{17}$$

Integrating eq 17 with initial condition $\tilde{Q}(\tilde{z}=0)=1$ results in

$$\tilde{Q}_{cr} = 1 - \frac{2\pi k H_f}{\mu Q_0(1+mt_{tr})}\frac{\Delta p}{\ln\frac{r_e}{r_w}}\tilde{z}_{cr} \tag{18}$$

The critical depth, $\tilde{z}_{cr}$, is determined using the expression for the critical rate (eq13)

$$\tilde{z}_{cr} = \frac{\mu Q_0(1+mt_{tr})}{2\pi k H_f \Delta p}\ln\frac{r_e}{r_w}\left(1 + D - C\left(\frac{A}{B}+1\right)^{4/3}\right) \tag{19}$$

The initial condition for the ordinary differential eq 12 in the case of high rate is formulated as

$$\tilde{z} = \tilde{z}_{cr}: \quad \tilde{h}_c = 0 \tag{20}$$

Separating variables in eq 12 and accounting for the initial condition (eq 20) yield

$$\tilde{z} - \tilde{z}_{cr} = \frac{1}{G}\left\{\frac{4C}{3}\int_{\tilde{h}_c}^{0}\left(\frac{A(-\ln(1-\tilde{h}_c)+B-1)}{(1-\tilde{h}_c)^2(-\ln(1-\tilde{h}_c)+B)}\right)\left(\frac{A}{(1-\tilde{h}_c)(-\ln(1-\tilde{h}_c)+B)}+1\right)^{1/3}(1-\tilde{h}_c)^3\,d\tilde{h}_c - 3\int_{\tilde{h}_c}^{0}\left[C\left(\frac{A}{(1-\tilde{h}_c)(-\ln(1-\tilde{h}_c)+B)}+1\right)^{4/3} - D\right][-\ln(1-\tilde{h}_c)+B](1-\tilde{h}_c)^2\,d\tilde{h}_c\right\} \tag{21}$$

In eq 21, C, D, and G are calculated from eqs 10 and 11 by replacing Q_0 and H_f with Q_{cr} and $H_f - z_{cr}$, respectively.

The analytical model in eqs 16 and 21 describes nonuniform cake profile formed by drag, electrostatic, permeate, and gravitational forces along with external surface stress torque. The calculations are presented in the next section.

5. EFFECTS OF PHYSICAL PARAMETERS ON CAKE PROFILE

In this Section, the analytical model (eqs 16 and 21) is used to investigate the effects of injection rate, cake porosity, particle Young's modulus and Poisson's ratio, pressure drawdown, and salinity on the cake thickness profile.

DOI: 10.1021/ie504936q
Ind. Eng. Chem. Res. 2015, 54, 3051−3061

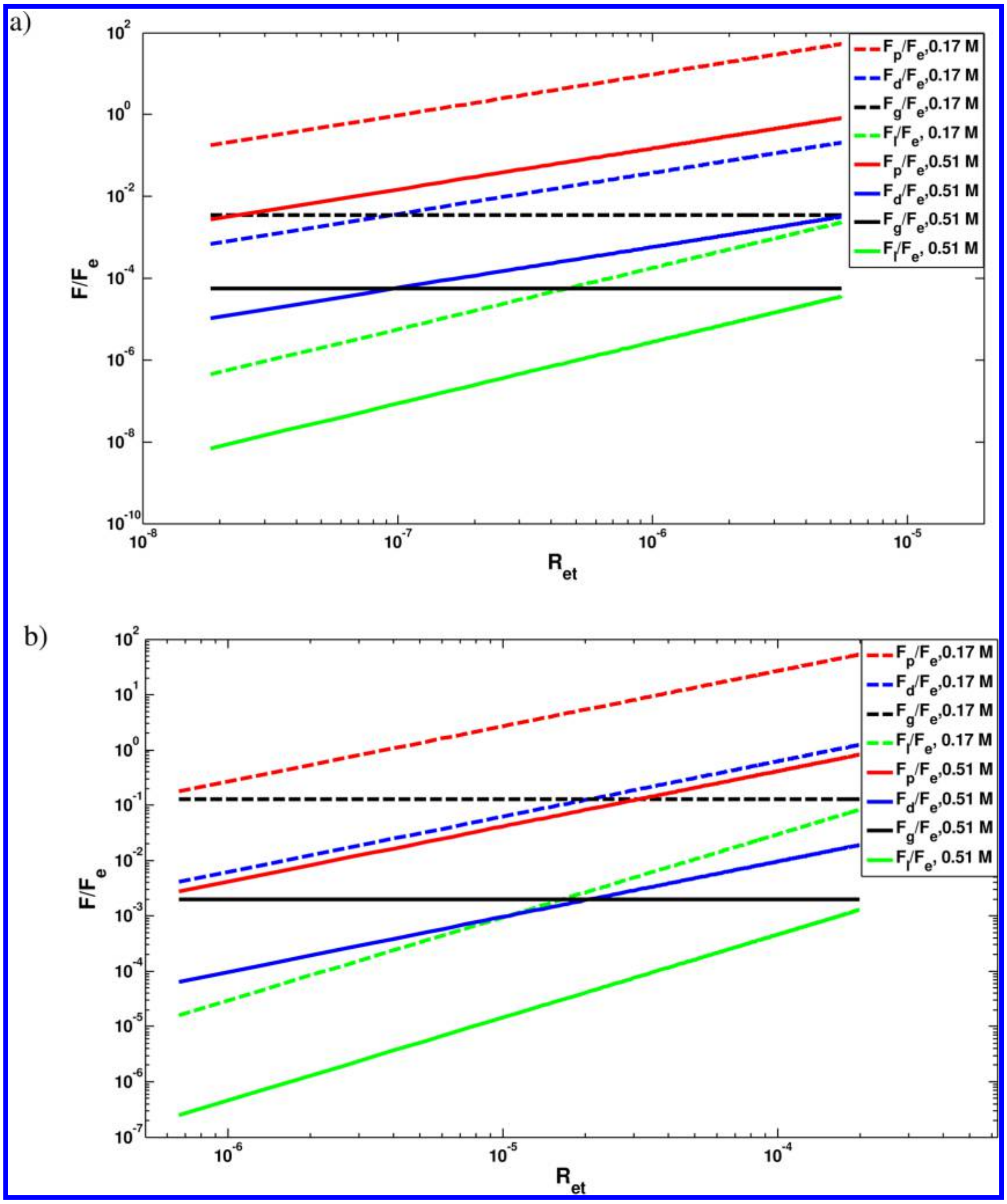

Figure 4. Ratio of permeate, drag, gravitational, and lifting forces to electrostatic force for (a) r_s = 0.5 μm and (b) r_s = 3 μm (μ = 0.001 Pa S; ρ_w = 1000 kg/m^3; ρ_s = 2600 kg/m^3; r_w = 0.1 m; ϕ_c = 0.1; H_f = 100 m; Q_0 = 1.157 × 10^{-4} to 0.0347 m^3/s).

The electrostatic force is calculated using DLVO theory (see S-1−S-7 in Appendix S1, Supporting Information). The following electrostatic constants are chosen for the conditions of seawater injection into a sandstone reservoir: Hamaker constant corresponds to quartz−quartz interaction in aqueous environment and sandstone reservoirs, $A_{132} = 2.0 \times 10^{-21}$ J (see refs 43−46); ζ-potentials for quartz particles and cake matter, $\zeta_1 = \zeta_2 = -12$ mV, correspond to seawater salinity of 0.51 M of Na^+ equivalent;[7,43,47] the permittivity of free space (vacuum) is $\varepsilon_0 = 8.854 \times 10^{-12}$ C^2 J^{-1} m^{-1}; $\varepsilon_r = 78.0$ is the relative permittivity for water (see Khilar and Fogler[7] and Elimelech et al.[47]); Boltzmann constant, $k_B = 1.3806504 \times 10^{-23}$ J/K; atomic collision diameter in Lennard-Jones potential is σ_{LJ} = 0.5 nm (Khilar and Fogler,[7] Das et al.[48]); the inverse Debye length, κ = 2.35 × 10^9 m^{-1}, is calculated by (eq S-7 in Supporting Information) for seawater with $Z = 1$ for sodium chloride and seawater salinity C_m = 510 mol/m^3. For the case of medium salinity of 0.17 M, the inverse Debye length becomes κ = 1.35 × 10^9 m^{-1}.

The total energy potential for electrostatic particle−rock interaction is shown in Figure 3 for high and medium salinities and two particle sizes. High salinity provides strong attraction for both size particles with favorable deposition conditions. The medium salinity also provides favorable conditions for particle deposition on the cake surface; however, the energy minimum is shallower, which leads to formation of thinner external filter cake.

DOI: 10.1021/ie504936q
Ind. Eng. Chem. Res. 2015, 54, 3051−3061

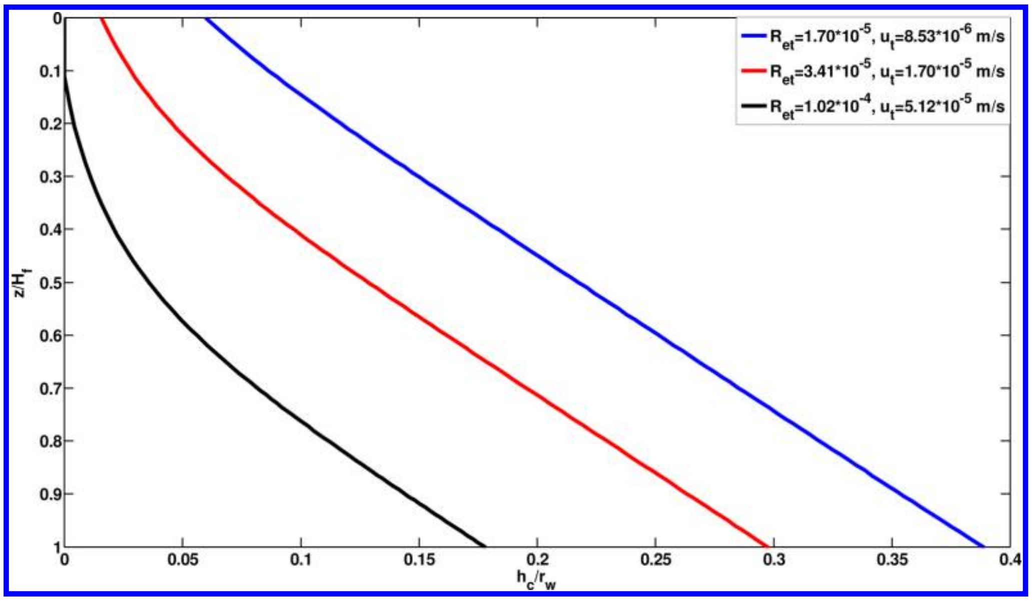

Figure 5. Effect of the injection rate on cake thickness profile.

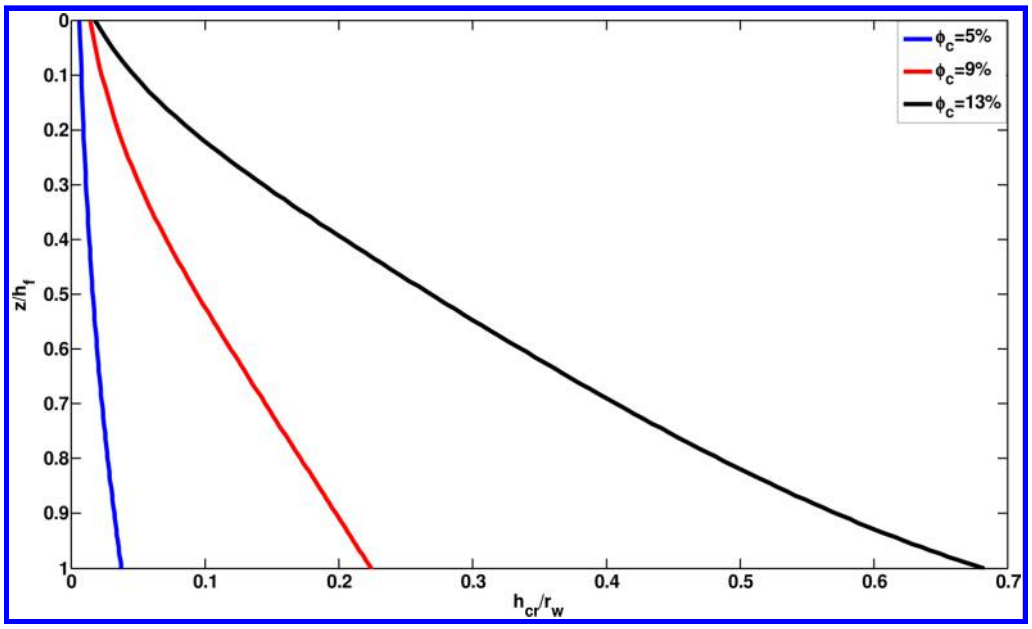

Figure 6. Effect of filter cake porosity on the cake thickness profile.

The tangential flux through a well cross-section is expressed via dimensionless particle Reynolds number, defined as

$$\mathrm{Re}_t = \frac{\rho_w u_t r_s}{\mu} \tag{22}$$

Figure 4 shows the comparison of permeate, drag, gravitational, and lifting forces with electrostatic force. When the well rate Q_0 varies from 1.157×10^{-4} to 0.0347 m^3/s, constant particle size r_s = 0.5 μm, water density ρ_w = 1000 kg/m^3, and viscosity μ = 0.001 Pa·s, Reynolds number varies from 2×10^{-8} to 6×10^{-6} (Figure 4a). For r_s = 3.0 μm, the Reynolds number varies from 7×10^{-6} to 2×10^{-4} (Figure 4b). Two salinities of seawater, 0.51 M and medium salinity 0.17 M, are considered. In this figure, tangential rate is assumed to be half of the injection rate because of rate variation along the injection interval.

For all the cases,the lifting force is negligible if compared with the electrostatic force. Because they both act in the same direction, the lifting force is neglected in the model for cake equilibrium (see eq 1). Gravitational force is negligible if compared with electrostatic force for all the cases except for the case of medium salinity and large particles; the ratio F_g/F_e varies from 10^{-4} to 10^{-1}. However, the lever arm for gravitational force exceeds that for normal force by 10^2−10^3 times, so the torque of gravitational force has the same order of magnitude as that of electrostatic force. Therefore, gravity must be accounted for in the mechanical equilibrium model (eq 1). Permeate and drag forces have the same order of magnitude as the electrostatic force.

Now let us analyze how the main factors affect the cake thickness and profile along the well. The following data are used for calculations: Q_0 = 0.0116 m^3/s, σ = 0.2, E = 40 GPa, r_s = 2 μm, H_f = 100 m, p_w = 27.6 MPa, p_{res} = 13.8 MPa, ρ_w = 1000 kg/m^3, ρ_s = 2600 kg/m^3, salinity = 0.51 M, $k = 10^{-13}$ m^2, k_c =

DOI: 10.1021/ie504936q
Ind. Eng. Chem. Res. 2015, 54, 3051−3061

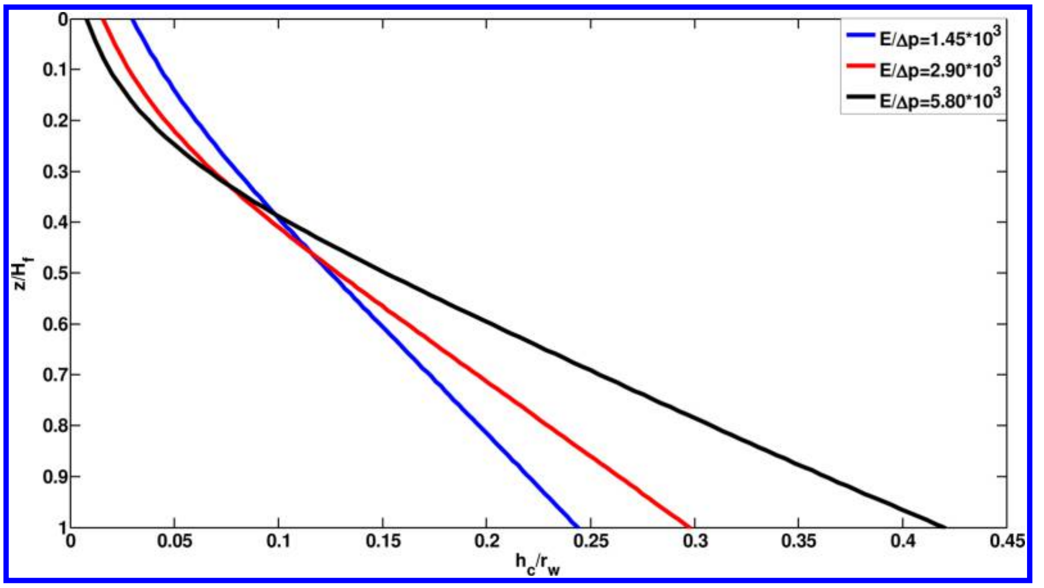

Figure 7. Effect of Young's modulus on cake thickness profile.

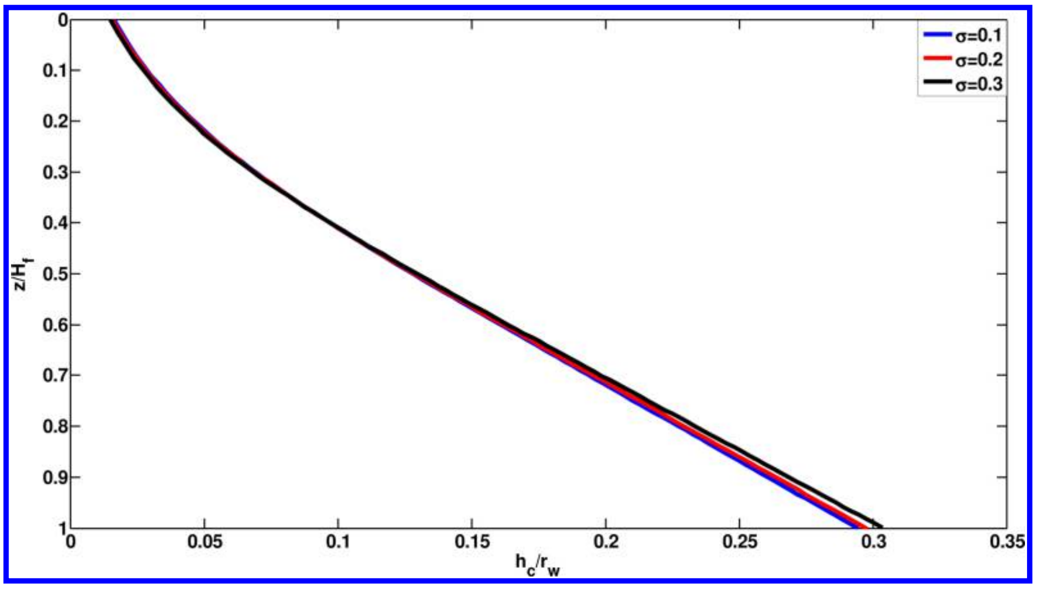

Figure 8. Effect of Poisson's ratio on cake thickness profile.

1.1×10^{-16} m^2, $\phi_c = 0.1$, $r_e = 500$ m, $r_w = 0.12$ m, $\mu = 0.001$ Pa·s, $\lambda = 25$ m^{-1}, $\beta = 300$, $\alpha = 0.09$, c^0=1 ppm, $\phi = 0.3$.

To investigate the effect of injection rate, Q_0, on the cake thickness, three values of injected rate are considered: Q_0 = 0.0058, 0.0116, and 0.0347 m^3/s. The injection rate increase causes the increase of detaching drag force (eq S-8 in Supporting Information) and attaching permeate force (eq S-10 in Supporting Information), exhibiting two competitive effects. However, Figure 5 shows that the higher injection rate leads to thinner filter cakes. Therefore, the effect of drag force dominates over the permeate force effect. This is explained by the low value of the lever arm ratio, l_n/l_d, causing higher torque for the detaching drag force.

Blue and red curves in Figure 5 correspond to injection rate lower than the critical value Q_{cr}. As a result, the cake is built up from the top of the reservoir $z/H_f = 0$. The critical rate, as calculated from eq 13, is equal to 0.025 m^3/s. The cake profile is determined from eq 16. The rate corresponding to the black curve is above the critical value; therefore, the cake is built up in the lower well section. The profile of cake is given by eq 21.

Figure 6 shows the effect of filter cake porosity on the cake thickness profile. Because small variation of particle form can significantly affect the cake porosity,[49] this effect is important for well behavior prediction. As follows from the calculations using the Kozeny−Carman equation[50,51] (eq S-12 in Supporting Information), increase in the cake porosity ϕ_c = 5%, 9%, and 13% corresponds to ratios $k_c/r_s^2 = 3.08 \times 10^{-6}$, 1.95×10^{-5}, and 6.45×10^{-5}, respectively. The increase of ratio k_c/r_s^2 can be interpreted as cake permeability increase under the same particle size. The higher the cake permeability, the larger the rate q, the greater the permeate force (eq S-10 in Supporting Information), and the thicker the cake. Simultaneously, the higher the rate q, the lower the tangential rate (Q), the smaller the drag force (eq S-8 in Supporting Information), and the thicker the cake, i.e., for the example considered, the effects of both forces cause the same result of thicker cake for greater cake porosity.

DOI: 10.1021/ie504936q
Ind. Eng. Chem. Res. 2015, 54, 3051−3061

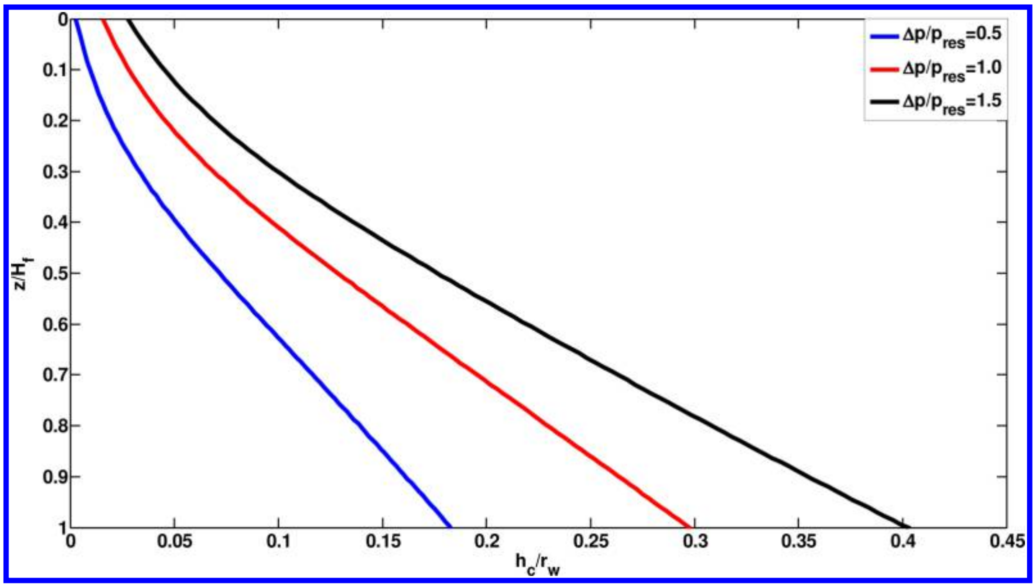

Figure 9. Effect of pressure difference on cake thickness profile.

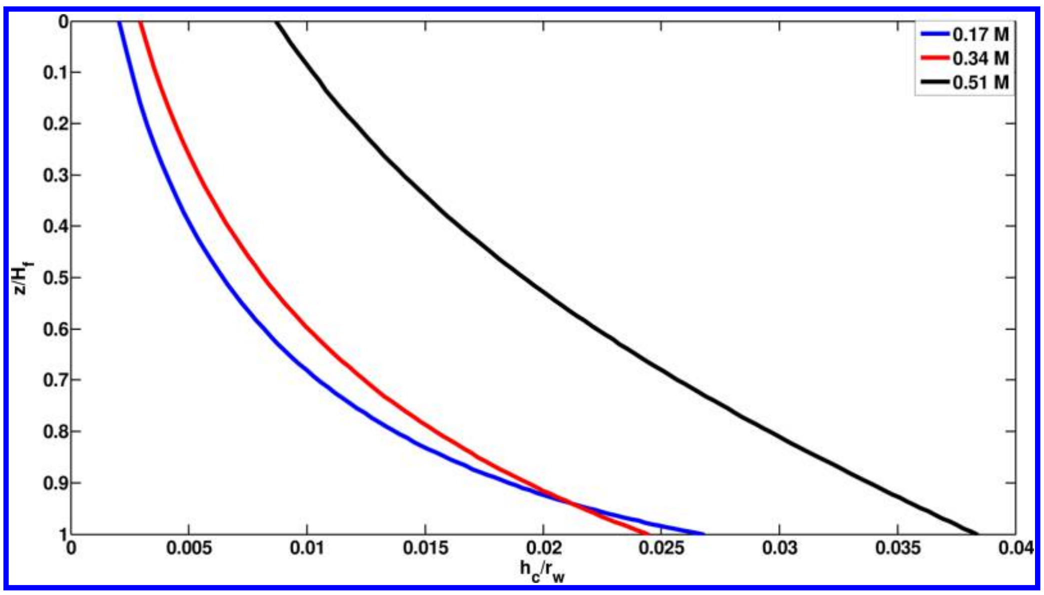

Figure 10. Effect of water salinity on cake thickness profile.

The effect of Young's modulus on cake thickness is presented in Figure 7. The cake profiles are compared for three Young's modulus values: 20, 40, and 80 GPa. The higher the Young's modulus, the smaller the contact deformation area size l_n (see refs 6 and 39−41), the smaller the attaching torque, and the thinner the cake. As shown in Figure 7, this effect takes place in the upper part of the well. In the lower well section, the cake thinning causes increase of the normal rate (q), decrease of tangential rate (Q), and reduction in the drag force (eq S-8 in Supporting Information). It results in a thicker cake profile.

The qualitative effect of Poisson's ratio on the cake profile is the same as that of Young's modulus. The greater the Poisson's ratio, the smaller the normal lever arm l_n (see refs 39−41). The black curve in Figure 8 is located below the other curves in the upper well section and above the other curves in the lower section of the well. However, the quantitative effect of Poisson's ratio on the cake thickness is negligible.

Figure 9 shows that the higher the pressure drawdown, the thicker the cake. Indeed, the increase of Δp results in higher normal rate, larger attaching permeate force (eq S-10 in Supporting Information), and thicker cake. Simultaneously, tangential rate decreases along with the drag force, leading to the thicker cake as well. The example studied in this work corresponds to water injection into the reservoir with intensive pressure depletion, where the drawdown increases under the constant injection rate.

Moreover, the increase of salinity leads to the increase of attractive attaching electrostatic force, resulting in the thicker cake. Figure 10 exhibits this effect in the upper well section. Three curves correspond to ζ-potentials of $\zeta_1 = \zeta_2 = -12$, -18, and -27 mV for salinities of 0.51, 0.34, and 0.17 M, respectively. On the other hand, the larger cake thickness results in a smaller normal rate (q), and a larger tangential rate (Q). This yields larger detaching drag force and thinner cake (blue curve is above the red one in the lower well section).

DOI: 10.1021/ie504936q
Ind. Eng. Chem. Res. 2015, 54, 3051−3061

6. DISCUSSION

The presented model assumes a homogeneous reservoir. However, the exact formulas presented in eqs 16 and 21 for cake profile can be extended for layer-cake reservoir $k = k(z)$ with isolated layers.

The developed model can be modified for the case of fractured injector. Assume constant pressure in the fracture and formation of the uniform cake with the constant thickness over the vertical. The flow in the reservoir near the fracture surface becomes one-dimensional and linear. The flow description has the same structure as eqs S-14–S-23 in Supporting Information, changing the axi-symmetric flow using coordinates (r, t) to the linear–parallel flow (x, t) (see ref 9). It changes the leak-off rate in eq 4 and expressions for permeate velocity in eq 7. The modified implicit solution (eq 21) presents cake thickness variation along the flow in the fracture.

Another approach to filter cake formation during the injection into fractured wells is proposed in ref 52. The model is developed for extrusion of the polymer gels during the injection and can be applied for formation of external filter cake during injection of water with solid particles. The traditional cake model assumes the formation of uniform cake on the fracture wall (see refs 10, 11, 26, 32, and 33), while the wormhole flow structure in the fracture is assumed in ref 52. The model describes formation and development of wormholes and their healing with time by newly injected particles. The flow and cake geometry in the wormhole model is essentially three-dimensional.

The main elements of the mathematical model (eqs 1–5)—torque balance as a condition for mechanical equilibrium of the cake, expressions for different forces and lever arm ratio, and Hertz's theory to determine the particle–rock contact area—are verified by the laboratory tests.[32,33] In previous papers on stabilized cake in "short" wells, the model has also been verified by the analysis of several oil field wells.[32,33] The only new element of the basic model for stabilized cake in "long" wells developed in the present work is a common volumetric balance (eq 4), which does not require validation.

However, the comparison between cake profiles as obtained from the mathematical modeling and from direct measurements in controlled laboratory experiments or in wells would significantly enhance the reliability of the developed model. Yet, to the best of our knowledge, the measurements of cake thickness variation in long wells are not available in the literature.

The cake profile along the well determines the well index; thus, its reliable modeling is important for well behavior prediction. However, the information about particle properties such as size, shape, Young's modulus, and Poisson's ratio is often unavailable under field conditions. Existence of numerous poorly determined model parameters makes the prediction unreliable. The formulation of the particular cases, where the number of model parameters can be reduced, increases the prediction reliability.

As is shown in section 5, the lifting force can be neglected, so the determination of the empirical lifting factor is not necessary.

As is shown in ref 32, the lever arms l_n and l_d in eq 1 are not randomly distributed as in the case of an asperous surface, but are defined by the elastic particle and rock properties. The normal lever arm (l_n) can be determined as a size of the contact deformation area using Hertz's theory. For high Young's modulus values that are typical for sandstone rocks and particles, the contact deformation area is small ($l_n \ll l_d$), allowing us to assume that the tangential lever arm (l_d) is equal to the particle size (r_s). The above speculations permit further decrease of the empirical model parameters by two.

7. CONCLUSIONS

Derivation of the equation for nonuniform cake profile in long wells accounting for electrostatic force, for varying permeate correction factor, and using Hertz's theory for lever arm ratio calculations allows us to draw the following conclusions:

- The forces affecting thickness of external filter cake are drag, electrostatic, permeate, and gravitational forces together with the external torque (moment). Lifting force can be neglected.
- Neglecting the lifting force yields reduction of the number of model coefficients by one (by the lifting factor).
- Using Hertz's contact deformation theory for calculation of the normal lever arm further decreases the number of model coefficients by one (by the normal lever arm) if compared with the torque model for asperities.
- For sandstone minerals with high Young's modulus, where the contact area size is significantly smaller than the particle radius, the tangential level arm is approximately equal to the particle radius, also yielding the reduction of the number of model constants by one (by the tangential lever arm).
- Nonuniform profile of external filter cake on well wall in thick reservoirs during water injection or drilling can be described by an implicit formula.
- There exists a critical well rate corresponding to zero cake thickness. If the rate is below the critical value, the external cake is built up in the overall injection interval. If the rate is above the critical value, there is no cake in the upper part of the wellbore; the cake starts at the depth where the tangential rate reaches the critical value.
- The most significant factors affecting cake thickness are injection rate, cake porosity, water salinity, and Young's modulus.

■ ASSOCIATED CONTENT

Ⓢ Supporting Information

Expressions for forces and derivation of equations for well inflow performance in the reservoir with rocks containing the retained particles and external filter cake on the well surface (Appendix S1, Forces and torques acting on a particle at the external cake surface; Appendix S2, Axi-symmetric steady-state flow toward well). This material is available free of charge via the Internet at http://pubs.acs.org.

■ AUTHOR INFORMATION

Corresponding Author

*E-mail: zhenjiang.you@adelaide.edu.au.

Notes

The authors declare no competing financial interest.

■ ACKNOWLEDGMENTS

The authors are grateful to Dr. Themis Carageorgos (Australian School of Petroleum) for help in English editing.

NOMENCLATURE

A_{132} = Hamaker constant, ML^2T^{-2}, J
C_m = Molar concentration of ith ion, mol L^{-3},mol m^{-3}
c^0 = Injected suspended particle concentration, ppm
E = Young's modulus, $ML^{-1}T^{-2}$, N m^{-2}
E_s = Young's modulus of solid particle, $ML^{-1}T^{-2}$, N m^{-2}
e = Electron charge, C
F_d = Drag force, MLT^{-2}, N
F_e = Electrostatic force, MLT^{-2}, N
F_g = Gravitational force, MLT^{-2}, N
F_l = Lifting force, MLT^{-2}, N
F_p = Permeate force, MLT^{-2}, N
h = Separation distance, L, m
h_c = Cake thickness, L, m
$\tilde{h}_c$ = Dimensionless stabilized cake thickness
$\tilde{h}_{c0}$ = Dimensionless stabilized cake thickness at $\tilde{z}$ = 0
H_f = Reservoir thickness, L, m
j = Impedance
K = Composite Young's modulus, $ML^{-1}T^{-2}$, N m^{-2}
k = Reservoir permeability, L^2, m^2
k_B = Boltzmann constant, $ML^2T^{-2}K^{-1}$
k_c = Cake permeability, L^2, m^2
l_d = Lever arm for tangential forces, L, m
l_n = Lever arm for normal forces, L, m
m = Slope of impedance growth during deep bed filtration
M_E = External moment, ML^2T^{-2}, N m
n_∞ = Bulk number density of ions, L^{-3}, m^{-3}
p_c = Pressure at $r = r_w$, $ML^{-1}T^{-2}$, N m^{-2}
p_{res} = Reservoir pressure, $ML^{-1}T^{-2}$, N m^{-2}
p_w = Well pressure, $ML^{-1}T^{-2}$, N m^{-2}
Q = Tangential rate along the well, L^3T^{-1}, m^3 s^{-1}
$\tilde{Q}$ = Dimensionless tangential rate along the well
Q_0 = Injection rate, L^3T^{-1}, m^3 s^{-1}
q = Permeate (normal) flow rate, L^3T^{-1}, m^3 s^{-1}
Re_t = Particle Reynolds number
r = Radius, L, m
r_e = Reservoir drainage radius, L, m
r_s = Particle radius, L, m
r_w = Well radius, L, m
T = Absolute temperature, K
t = Time, T, s
t_{tr} = Dimensionless transition time (PVI)
u_p = Permeate velocity, L T^{-1}, m s^{-1}
u_t = Tangential velocity at particle center, LT^{-1}, m s^{-1}
V = Energy of interaction, ML^2T^{-2}, J
Z_i = Valence of ith ion
z = Distance from top of the reservoir, L, m
$\tilde{z}$ = Dimensionless distance from top of the reservoir

Greek letters

α = Critical porosity fraction
β = Formation damage coefficient
ε_r = Relative permittivity of water
ε_0 = Free space permittivity, $C^2J^{-1}L^{-1}$
κ = Inverse Debye length, L^{-1}, m^{-1}
λ = Filtration coefficient, L^{-1}, m^{-1}
λ_{cw} = Characteristic wavelength of interaction, L, m
μ = Dynamic viscosity, $ML^{-1}T^{-1}$, kg $m^{-1}s^{-1}$
ν_i = Number concentration of ith ion, L^{-3}, m^{-3}
σ = Poisson's ratio
σ_s = Poisson's ratio of solid particle
σ_{LJ} = Atomic collision diameter, L, m
ρ_w = Water density, ML^{-3}, kg m^{-3}
ρ_s = Particle density, ML^{-3}, kg m^{-3}
Δp = Pressure drawdown, $ML^{-1}T^{-2}$, N m^{-2}
$\Delta\rho$ = Density difference between particle and water, ML^{-3}, kg m^{-3}
σ_{LJ} = Atomic collision diameter, L, m
ϕ = Porosity
Φ_H = Permeate force factor
ζ = Zeta potential, ML^2T^{-2}, mV
ω = Drag force coefficient

Abbreviation

PVI = Pore volume injected

Subscripts

BR = Born repulsion (for energy potential)
c = Cake
cr = Critical
d = Drag
DLR = Double layer repulsion (for energy potential)
e = Electric
g = Gravity
l = Lifting
i = Index for ions
LVA = London−van der Waals (for energy potential)
n = Normal
p = Permeate
res = Reservoir
s = Solid particle
w = Well
0 = Initial condition (boundary value)

REFERENCES

(1) Cheng, A. H. -D.; Benhachmi, M. K.; Halhal, D.; Ouazar, D.; Naji, A.; EL Harrouni, K. Pumping Optimization in Saltwater-Intruded Aquifers. In *Coastal Aquifer Management-Monitoring, Modeling, and Case Studies*; Cheng, A. H.-D., Ouazar, D., Eds.; CRC Press: Boca Raton, FL, 2004; pp 178−196.

(2) Cheng, A. H. -D.; Halhal, D.; Naji, A.; Ouazar, D. Pumping Optimization in Saltwater-Intruded Coastal Aquifers. *Water Resour. Res.* **2000**, *36*, 2155.

(3) Bear, J. Conceptual and Mathematical Modeling. In *Seawater Intrusion in Coastal Aquifers-Concepts, Methods and Practices*; Bear, J., Cheng, A. H.-D., Sorek. S., Ouazar. D., Herrera, I., Eds.; Kluwer Academic Publishers: Dordrecht, 1999; pp 127−161.

(4) Rosenbrand, E.; Haugwitz, C.; Jacobsen, P. S. M.; Kjøller, C.; Fabricius, I. L. The Effect of Hot Water Injection on Sandstone Permeability. *Geothermics* **2014**, *50*, 155.

(5) Civan, F. *Reservoir Formation Damage: Fundamentals, Modeling, Assessment, and Mitigation*, 2nd ed.; Gulf Professional Publishing: Burlington, MA, 2007.

(6) Schechter, R. S. *Oil Well Stimulation*; Prentice Hall: Englewood Cliffs, NJ, 1992.

(7) Khilar, K. C.; Fogler, H. S. *Migration of Fines in Porous Media*; Kluwer Academic Publishers: Dordrecht, 1998.

(8) Bedrikovetsky, P. *Mathematical Theory of Oil and Gas Recovery: With Applications to ex-USSR Oil and Gas Fields*; Kluwer Academic Publishers: Dordrecht, 1993.

(9) Herzig, J. P.; Leclerc, D. M.; Le Goff, P. Flow of Suspensions through Porous Media—Application to Deep Filtration. *Ind. Eng. Chem.* **1970**, *62*, 8.

(10) Pang, S.; Sharma, M. M. A Model for Predicting Injectivity Decline in Water Injection Wells. *SPE Form. Eval.* **1997**, *12*, 194, http://dx.doi.org/10.2118/28489-PA.

(11) Sharma, M. M.; Pang, S.; Wennberg, K. E.; Morgenthaler, L. N. Injectivity Decline in Water-Injection Wells: An Offshore Gulf of Mexico Case Study. *SPE Prod. Facil.* **2000**, *15*, 6, http://dx.doi.org/10.2118/60901-PA.

DOI: 10.1021/ie504936q
Ind. Eng. Chem. Res. 2015, 54, 3051−3061

(12) Sacramento, R. N.; Yang, Y.; You, Z.; Waldmann, A.; Martins, A. L.; Vaz, A. S. L.; Zitha, P. L. J.; Bedrikovetsky, P. Deep Bed and Cake Filtration of Two-Size Particle Suspension in Porous Media. *J. Pet. Sci. Eng.* **2015**, *126*, 201.

(13) Bedrikovetsky, P.; Marchesin, D.; Shecaira, F.; Souza, A. L.; Milanez, P. V.; Rezende, E. Characterization of Deep Bed Filtration System from Laboratory Pressure Drop Measurements. *J. Pet. Sci. Eng.* **2001**, *32*, 167.

(14) Cortis, A.; Harter, T.; Hou, L.; Atwill, E. R.; Packman, A. I.; Green, P. G. Transport of *Cryptosporidium parvum* in Porous Media: Long-Term Elution Experiments and Continuous Time Random Walk Filtration Modeling. *Water Resour. Res.* **2006**, *42*, W12S13 DOI: 10.1029/2006WR004897.

(15) Shapiro, A. A. Elliptic Equation for Random Walks. Application to Transport in Microporous Media. *Phys. A (Amsterdam, Neth.)* **2007**, *375*, 8.

(16) Lin, H.-K.; Pryadko, L. P.; Walker, S.; Zandi, R. Attachment and Detachment Rate Distributions in Deep-Bed Filtration. *Phys. Rev. E: Stat., Nonlinear, Soft Matter Phys.* **2009**, *79*, 046321-1 DOI: 10.1103/PhysRevE.79.046321.

(17) Yuan, H.; Shapiro, A. A. Modeling Non-Fickian Transport and Hyperexponential Deposition for Deep Bed Filtration. *Chem. Eng. J. (Amsterdam, Neth.)* **2010**, *162*, 974.

(18) Sharma, M. M.; Yortsos, Y. C. Transport of Particulate Suspensions in Porous Media: Model Formulation. *AIChE J.* **1987**, *33*, 1636.

(19) Sharma, M. M.; Yortsos, Y. C. A Network Model for Deep Bed Filtration Processes. *AIChE J.* **1987**, *33*, 1644.

(20) Sharma, M. M.; Yortsos, Y. C. Fines Migration in Porous Media. *AIChE J.* **1987**, *33*, 1654.

(21) Bedrikovetsky, P. Upscaling of Stochastic Micro Model for Suspension Transport in Porous Media. *Transp. Porous Media* **2008**, *75*, 335.

(22) Yuan, H.; Shapiro, A.; You, Z.; Badalyan, A. Estimating Filtration Coefficients for Straining from Percolation and Random Walk Theories. *Chem. Eng. J. (Amsterdam, Neth.)* **2012**, *210*, 63.

(23) Payatakes, A. C.; Tien, C.; Turian, R. M. A New Model for Granular Porous Media. I. Model Formulation. *AIChE J.* **1973**, *19*, 58.

(24) Payatakes, A. C.; Rajagopalan, R.; Tien, C. Application of Porous Media Models to the Study of Deep Bed Filtration. *Can. J. Chem. Eng.* **1974**, *52*, 722.

(25) Bradford, S. A.; Kim, H. N.; Haznedaroglu, B. Z.; Torkzaban, S.; Walker, S. L. Coupled Factors Influencing Concentration-Dependent Colloid Transport and Retention in Saturated Porous Media. *Environ. Sci. Technol.* **2009**, *43*, 6996.

(26) Ochi, J.; Detienne, J. L., Rivet, P.; Lacourie, Y. External Filter Cake Properties During Injection of Produced Waters. Presented at SPE European Formation Damage Conference, The Hague, Netherlands, May 31−June 1, 1999; Paper SPE 54773. ISBN: 978-1-55563-361-5.

(27) Ramarao, B. V.; Tien, C. Approximate Analysis of Fine-Particle Retention in the Cake Filtration of Suspensions. *Ind. Eng. Chem. Res.* **2005**, *44*, 1424.

(28) Tien, C. *Introduction to Cake Filtration: Analyses, Experiments and Applications*; Elsevier: Amsterdam, 2006.

(29) Freitas, A. M.; Sharma, M. M. Detachment of Particles from Surfaces: An AFM Study. *J. Colloid Interface Sci.* **2001**, *233*, 73.

(30) Jiao, D.; Sharma, M. M. Mechanism of Cake Buildup in Crossflow Filtration of Colloidal Suspensions. *J. Colloid Interface Sci.* **1994**, *162*, 454.

(31) Civan, F. Incompressive Cake Filtration: Mechanism, Parameters, and Modeling. *AIChE J.* **1998**, *44*, 2379.

(32) Kalantariasl, A.; Bedrikovetsky, P. Stabilization of External Filter Cake by Colloidal Forces in a "Well-Reservoir" System. *Ind. Eng. Chem. Res.* **2014**, *53*, 930.

(33) Kalantariasl, A.; Zeinijahromi, A.; Bedrikovetsky, P. Axi-Symmetric Two-Phase Suspension-Colloidal Flow in Porous Media during Water Injection. *Ind. Eng. Chem. Res.* **2014**, *53*, 15763.

(34) Zinati, F. F.; Farajzadeh, R.; Currie, P. K.; Zitha, P. L. J. Modeling of External Filter Cake Build-Up in Radial Geometry. *Pet. Sci. Technol.* **2009**, *27*, 746.

(35) Sherwood, J. D. The Force on a Sphere Pulled away from a Permeable Half-Space. *PhysicoChem. Hydrodyn.* **1988**, *10*, 3.

(36) Al-Abduwani, F. A. H.; Bedrikovetsky, P.; Farajzadeh, R.; van den Broek, W. M. G. T.; Currie, P. K. External Filter Cake Erosion: Mathematical Model and Experimental Study. Presented at SPE European Formation Damage Conference, Scheveningen, The Netherlands, May 25−27, 2005; Paper SPE 94635. ISBN: 978-1-55563-998-3.

(37) Bedrikovetsky, P.; Siqueira, F. D.; Furtado, C. A.; Souza, A. L. S. Modified Particle Detachment Model for Colloidal Transport in Porous Media. *Transp. Porous Media* **2011**, *86*, 353.

(38) Bedrikovetsky, P.; Zeinijahromi, A.; Siqueira, F. D.; Furtado, C. A.; Souza, A. L. S. Particle Detachment under Velocity Alternation during Suspension Transport in Porous Media. *Transp. Porous Media* **2012**, *91*, 173.

(39) Bergendahl, J. A.; Grasso, D. Mechanistic Basis for Particle Detachment from Granular Media. *Environ. Sci. Technol.* **2003**, *37*, 2317.

(40) Bergendahl, J.; Grasso, D. Prediction of Colloid Detachment in a Model Porous Media: Hydrodynamics. *Chem. Eng. Sci.* **2000**, *55*, 1523.

(41) Bradford, S. A.; Torkzaban, S.; Shapiro, A. A Theoretical Analysis of Colloid Attachment and Straining in Chemically Heterogeneous Porous Media. *Langmuir* **2013**, *29*, 6944.

(42) Derjaguin, B. V.; Muller, V. M.; Toporov, Y. P. Effect of Contact Deformations on The Adhesion of Particles. *J. Colloid Interface Sci.* **1975**, *53*, 314.

(43) Israelachvili, J. *Intermolecular and Surface Forces*, 3rd ed.; Academic Press: Amsterdam, 2011.

(44) Zhang, P.; Fan, C.; Lu, H.; Kan, A. T.; Tomson, M. B. Synthesis of Crystalline-Phase Silica-Based Calcium Phosphonate Nanomaterials and Their Transport in Carbonate and Sandstone Porous Media. *Ind. Eng. Chem. Res.* **2011**, *50*, 1819.

(45) Ishigami, T.; Fuse, H.; Asao, S.; Saeki, D.; Ohmukai, Y.; Kamio, E.; Matsuyama, H. Permeation of Dispersed Particles through a Pore and Transmembrane Pressure Behavior in Dead-End Constant-Flux Microfiltration by Two-Dimensional Direct Numerical Simulation. *Ind. Eng. Chem. Res.* **2013**, *52*, 4650.

(46) Kim, A. S.; Liu, Y. Irreversible Chemical Potential and Shear-Induced Diffusion in Cross-Flow Filtration. *Ind. Eng. Chem. Res.* **2008**, *47*, 5611.

(47) Elimelech, M.; Gregory, J.; Jia, X.; Williams, R. A. *Particle Deposition and Aggregation: Measuremnt, Modelling and Simulation*; Butterworth-Heinemann: Boston, 1995.

(48) Das, S. K.; Schechter, R. S.; Sharma, M. M. The Role of Surface Roughness and Contact Deformation on the Hydrodynamic Detachment of Particles from Surfaces. *J. Colloid Interface Sci.* **1994**, *164*, 63.

(49) Khatib, Z. I. Prediction of Formation Damage Due to Suspended Solids: Modeling Approach of Filter Cake Buildup in Injectors. Presented at SPE Annual Technical Conference and Exhibition, New Orleans, Louisiana, Sep. 25−28, 1994; Paper SPE 28488. ISBN: 978-1-55563-463-6.

(50) Lake, L. W. *Enhanced Oil Recovery*; Prentice Hall: Englewood Cliffs, NJ, 1989.

(51) Barenblatt, G. I.; Entov, V. M.; Ryzhik, V. M. *Theory of Fluid Flows through Natural Rocks*; Kluwer Academic Publishers: Dordrecht, 1990.

(52) Seright, R. S. An Alternative View of Filter-Cake Formation in Fractures Inspired by Cr(III)-Acetate-HPAM Gel Extrusion. *SPE Prod. Facil.* **2003**, *18*, 65, http://dx.doi.org/10.2118/81829-PA.

DOI: 10.1021/ie504936q
Ind. Eng. Chem. Res. 2015, 54, 3051−3061